

XY-Cut++: Advanced Layout Ordering via Hierarchical Mask Mechanism on a Novel Benchmark

Shuai Liu¹, Youmeng Li^{1*}, Jizeng Wei¹

¹College of Intelligence and Computing, Tianjin University, Tianjin, 300350, China.

*Corresponding author(s). E-mail(s): liyoumeng@tju.edu.cn;
Contributing authors: shuai.liu@tju.edu.cn; weijizeng@tju.edu.cn;

Abstract

Document Reading Order Recovery is a fundamental task in document image understanding, playing a pivotal role in enhancing Retrieval-Augmented Generation (RAG) and serving as a critical preprocessing step for large language models (LLMs). Existing methods often struggle with complex layouts (e.g., multi-column newspapers), high-overhead interactions between cross-modal elements (visual regions and textual semantics), and a lack of robust block-level evaluation benchmarks. We introduce **XY-Cut++**, an advanced layout ordering method that integrates pre-mask processing, multi-granularity segmentation, and cross-modal matching to address these challenges. Our method significantly enhances layout ordering accuracy compared to traditional XY-Cut techniques. Specifically, XY-Cut++ achieves **state-of-the-art** performance (98.8 BLEU overall) while maintaining simplicity and efficiency. It outperforms existing baselines by up to 24% and demonstrates consistent accuracy across simple and complex layouts on the newly introduced **DocBench-100** dataset. This advancement establishes a reliable foundation for document structure recovery, setting a new standard for layout ordering tasks and facilitating more effective RAG and LLM preprocessing.

Keywords: Document reading order, Document layout analysis, XY-Cut++, DocBench-100

1 Introduction

Document Reading Order Recovery is a fundamental task in document image understanding, serving as a cornerstone for enhancing Retrieval-Augmented Generation (RAG) systems and enabling high-quality data preprocessing for large language models (LLMs). Accurate layout recovery is essential for applications such as digital publishing and knowledge base construction. However, this task faces several significant challenges: (1) complex layout structure (e.g., multi-column layout, nested text boxes, non-rectangular text regions, cross-page content), (2) inefficient cross-modal alignment due to the high computational costs of integrating visual and textual features, and (3) the lack of standardized evaluation protocols for block-level reading order. Traditional approaches like XY-Cut [1] fail to model semantic dependencies in complex designs, while deep learning methods such as LayoutReader [2] suffer from prohibitive latency, limiting real-world deployment. Compounding these issues, existing datasets like ReadingBank [2] focus on word-level sequence annotations, which inadequately evaluate block-level structural reasoning—a necessity for real-world layout recovery. Although OmniDocBench [3] recently introduced block-level analysis support, its coverage of diverse complex layouts (e.g., newspapers, technical reports) remains sparse, further hindering systematic progress. Meanwhile, large-scale layout datasets such as DocBank [4] and PubLayNet [5] have advanced document layout analysis but primarily target word/line-level or scientific article layouts and do not directly benchmark block-level reading order.

To address these challenges, we propose XY-Cut++, an advanced framework for layout ordering that incorporates three core innovations: (a) pre-mask processing to mitigate interference from high-dynamic-range elements (e.g., title, figure, table), (b) multi-granularity region splitting for the adaptive decomposition of diverse layouts, and (c) lightweight cross-modal matching leveraging minimal semantic cues. Our approach significantly outperforms traditional methods in layout ordering accuracy. Additionally, we introduce

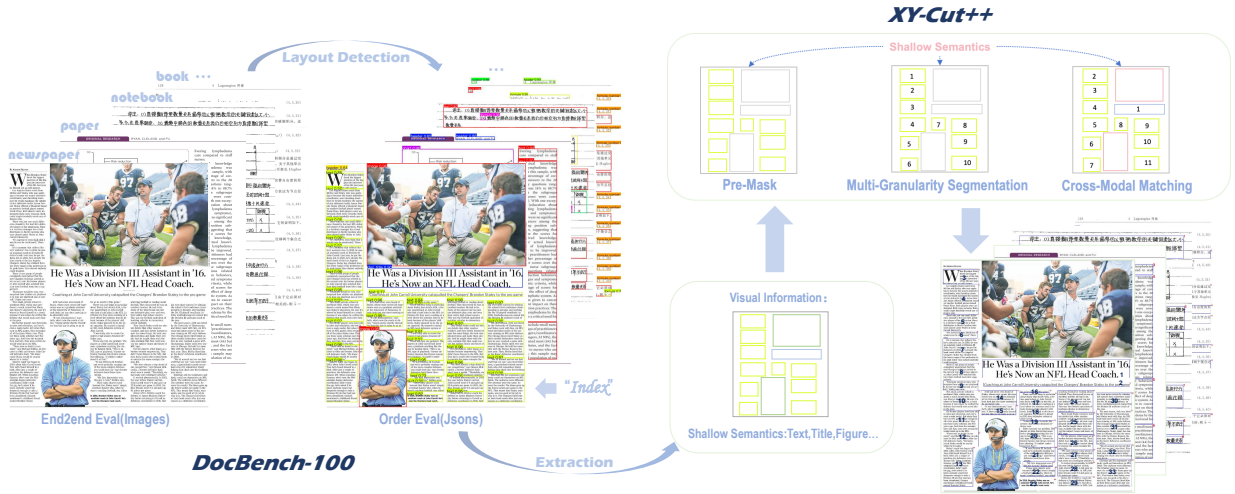


Fig. 1 XY-Cut++ Architecture with Hierarchical Mask Mechanism and DocBench-100 Benchmark. (left) DocBench-100 dataset composition and dual evaluation protocols. (right) Algorithm workflow integrating adaptive pre-mask processing, multi-granularity segmentation, and cross-modal matching.

DocBench-100, a novel benchmark dataset designed for evaluating layout ordering techniques. It includes 100 pages (30 complex and 70 regular layouts) with block-level reading order annotations. Extensive experiments on DocBench-100 demonstrate that our method achieves state-of-the-art performance. Specifically, our method achieves BLEU-4 scores of 98.6 (complex) and 98.9 (regular), surpassing baselines by 24% on average while maintaining $1.06\times$ FPS of geometric-only approaches.

The contributions of this paper are summarized as follows:

1. We present a simple yet high-performance enhanced XY-Cut framework that fuses shallow semantics and geometry awareness to achieve accurate layout ordering.
2. We curate DocBench-100, a block-level benchmark with diverse complex layouts that complements existing datasets and directly targets reading-order evaluation.
3. We achieved state-of-the-art results on both existing and new block-level datasets, and provided extensive ablations to each component in our methods.

2 Related Work

Document Reading Order Recovery has advanced from early heuristic rule-based methods to modern deep learning models, yet reliably handling complex layouts remains challenging.

2.1 Traditional Approaches

The XY-Cut algorithm [1] is a foundational technique in Document Reading Order Recovery that recursively divides documents into smaller regions based on horizontal and vertical projections. As illustrated in Figure 2, while it is effective for simple layouts, it struggles with complex structures, leading to inaccuracies

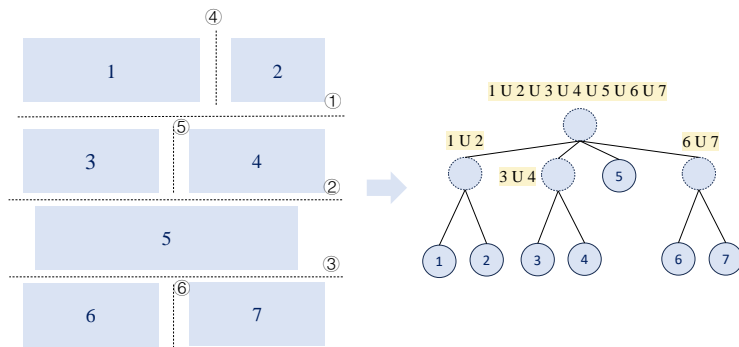


Fig. 2 XY-Cut Recursive Partitioning Workflow and Failure Analysis in Complex Layouts: (1) Initial document segmentation steps, (2) Connectivity assumption violations caused by cross-layout cell structures (cell 5), and (3) Error propagation through subsequent layout ordering. The correct reading order is 1, 3, 2, 4, 5, 6, 7.

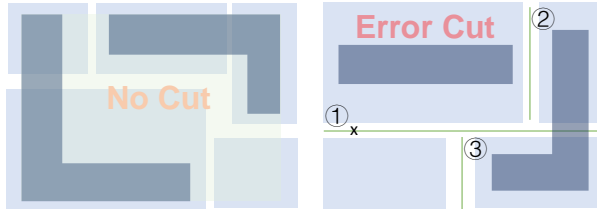


Fig. 3 Challenges posed by L-shaped inputs: (1) segmentation failure due to the inability to process L-shaped structures, and (2) missegmentation caused by improper handling of L-shaped regions. The correct sequence of segmentation is ②+③ ①.

in reading order recovery. Specifically, the rigid threshold mechanisms of XY-Cut can introduce hierarchical errors when handling intricate layouts, resulting in suboptimal performance. To address these limitations, various enhancements have been proposed. For instance, dynamic programming optimizations [6] have been introduced to improve segmentation stability. Additionally, mask-based normalization techniques [7] have been developed to mitigate some of the challenges associated with complex layouts. However, these improvements are still insufficient for handling intricate layouts and cross-page content. In our analysis of the XY-Cut algorithm, as discussed in [6, 7] and illustrated in Figure 3, we identified that many challenging cases arise from L-shaped inputs. A straightforward solution involves initially masking these L-shaped regions and subsequently restoring them. Upon implementing this approach, we found it to be remarkably effective while maintaining both simplicity and efficiency.

2.2 Deep Learning Approaches

Recent advances in Document Reading Order Recovery have been driven by deep learning models that effectively leverage multimodal cues. The LayoutLM series [8–12] pioneered the integration of textual semantics with 2D positional encoding, where LayoutLMv2 [9] introduced spatially aware pre-training objectives for cross-modal alignment and LayoutLMv3 [10] further unified text/image embeddings through self-supervised masked language modeling and image-text matching. LayoutXLM [11] extended this framework to multilingual document understanding. XYLayoutLM [12] advanced the field with its Augmented XY-Cut algorithm and Dilated Conditional Position Encoding, addressing variable-length layout modeling and generating reading order-aware representations for enhanced document understanding. Building upon these foundations, LayoutReader [2] demonstrated the effectiveness of deep learning in explicit reading order prediction through the sequential modeling of paragraph relationships. Critical to these advancements are large-scale datasets like DocBank [4], which provides weakly supervised layout annotations for fine-grained spatial modeling, and PubLayNet [5], which contains over 360,000 scientific document pages with hierarchical labels that encode implicit reading order priors through structural patterns. Specialized benchmarks like TableBank [13] further address domain-specific challenges by preserving the ordering of tabular data for table structure recognition.

Architectural innovations have significantly enhanced spatial reasoning capabilities. DocRes [14] introduces dynamic task-specific prompts (DTSPrompt), enabling the model to perform various document restoration tasks, such as dewarping, deshadowing, and appearance enhancement, meanwhile improving the overall readability and structure of documents. [15] iteratively aggregates features across different layers and resolutions, resulting in more refined feature representations that are beneficial for complex layout analysis tasks. By leveraging Hierarchical Document Analysis (HDA), models can more effectively capture intricate structural relationships within documents, facilitating more accurate predictions of reading order. Furthermore, advancements in unsupervised learning methods, such as those employed in DocUNet [16], have enabled more effective handling of document distortions, thereby enhancing OCR performance and layout analysis accuracy. DocFormer [17] unified text, visual, and layout embeddings through transformer fusion, improving contextual understanding for logical flow prediction. Complementary to these approaches, EAST [18] established robust text detection through geometry-aware frameworks, serving as a critical preprocessing step for element-level sequence derivation.

2.3 Benchmarks for Document Reading Order Recovery

Document Reading Order Recovery has seen significant advancements with deep learning models like LayoutLM [8] and LayoutReader [2], which integrate visual and textual features for tasks such as reading order prediction. However, existing methods face critical limitations in handling complex layouts (e.g., multi-column structures, cross-page content). A key challenge is the lack of benchmarks that directly evaluate block-level reading order, which is essential for applications like document digitization. While datasets such as ReadingBank [2] provide word-level annotations for predicting reading sequences, their design complicates the evaluation of methods focused on block-level performance. Specifically, word-level sequence annotations

Table 1 DocBench-100 subset statistics by column structure. Percentages are computed within each subset.

Subset	Pages	Single	Double	≥ 3
D_c	30	3.3%	6.7%	90.0%
D_r	70	38.6%	54.4%	7.0%

cannot simplify the assessment of dependencies between text blocks (e.g., the order of paragraphs or figures spanning multiple columns), which are essential for modeling complex layouts. Recently, OmniDocBench [3] has supported block-level analysis but suffers from limited coverage of complex layouts and sparse representation of domain-specific layouts (e.g., newspapers). To address these gaps, we introduce DocBench-100, which offers a broader range of layout structures and explicit metrics for assessing reading order accuracy, thereby enabling robust benchmarking of layout recovery systems.

3 DocBench-100 Dataset

To enable rigorous evaluation of block-level reading order, we construct DocBench-100, a curated benchmark emphasizing diverse real-world layouts. It complements existing datasets (ReadingBank [2], OmniDocBench [3], DocBank [4], PubLayNet [5]) by focusing on page-level block ordering across complex structures.

3.1 Sources and Composition

We source candidate pages from public document detection corpora (notably PP-DocLayout [19]) and MinerU [20] extraction outputs, then select pages exhibiting challenging phenomena: multi-column articles, irregular or spanning titles, interleaved figures/captions, and nested regions. The dataset comprises 100 pages split into: complex (D_c , 30 pages) and regular (D_r , 70 pages), following the prevalence in practical applications. An overview will be presented in Figure 4.

3.2 Fields and File Structure

Each page includes an image and two JSON files: (1) an input JSON (No Index) with fields `page_id`, `page_size`, `bbox`, `label`; (2) a GT JSON that additionally includes block-level reading order `index`. This design supports both end-to-end and oracle-detection evaluation protocols.

3.3 Annotation Pipeline

We adopt a two-stage pipeline:

- **Automatic pre-annotation:** MinerU [20] provides initial blocks, labels, and an order hypothesis.
- **Manual verification and screening:** Annotators correct segmentation and labels, and assign final `index`. Pages with inherently ambiguous global reading order (e.g., collage-like scans lacking semantic anchors) are excluded. All remaining reading orders are manually verified.

3.4 Statistics and Usage Protocols

D_c contains predominantly multi-column layouts (≥ 3 columns) and irregular titles, while D_r is dominated by single/double columns common in academic and business documents. Summary statistics by column structure are reported in Table 1. We recommend reporting both: (a) end-to-end image-based evaluation (requires detection) and (b) JSON-based evaluation on block sequences. We will release the evaluation script for block-level BLEU and dataset documentation.

4 Methods

Our geometry–semantic fusion pipeline (Figure 5) has four stages: (1) PP-DocLayout [19] extracts visual features and shallow semantic labels; (2) highly dynamic elements (e.g., titles, tables, figures) are pre-masked to alleviate the L-shape problem; (3) cross-layout elements are identified via global analysis, then processed with masking, real-time density estimation, and heuristic sorting; and (4) masked elements are re-mapped using nearest IoU edge-weighted margins. This geometry-aware pipeline with shallow semantics attains state-of-the-art results on DocBench-100 and OmniDocBench [3].



Fig. 4 DocBench-100 image overview: (a) 70-page regular subset D_r , and (b) 30-page complex subset D_c . All pages provide block-level reading-order ground truth for benchmarking layout-ordering methods.

4.1 Pre-Mask Processing

Our Pre-Masking mechanism is designed to reduce the interference of highly dynamic elements (e.g., figures and tables) on core block sorting. These elements can appear anywhere in documents with high positional flexibility, which may disrupt sorting logic. Specifically, we first identify such elements using shallow semantic labels from the PP-DocLayout detection model. We then build a binary mask to temporarily exclude these elements from subsequent multi-granularity segmentation and core block sorting. After multi-granularity sorting, we remap the masked elements back to the ordered layout in the cross-modal matching phase, using an IoU-weighted distance nearest-neighbor strategy. This two-stage "mask-then-remap" pipeline effectively separates highly dynamic elements from the key sorting stage, ensuring accurate core block ordering while maintaining layout fidelity, and also reduces the previously mentioned "L"-shaped input issues.

4.2 Multi-Granularity Segmentation

As shown in Figure 6, our hybrid segmentation framework integrates cross-layout element masking, geometric pre-segmentation, and density-driven adaptive refinement in three key phases. Each phase targets specific layout challenges, enabling robust segmentation for both regular and complex documents.

Phase 1: Cross-Layout Detection We first compute the document-level median bounding box length to establish an adaptive threshold for cross-layout elements (e.g., cross-column text spanning multiple grid units). Each content block B_i is represented by a 4-tuple (x_1, y_1, x_2, y_2) , where (x_1, y_1) is the top-left corner and (x_2, y_2) is the bottom-right corner. Let $\{l_i\}_{i=1}^N$ denote the length of each content bounding box B_i : for horizontal-layout documents (commonly used in daily scenarios, e.g., reports, articles), $l_i = x_{2,i} - x_{1,i}$ (horizontal width); for vertical-layout documents (e.g., classical Chinese texts), $l_i = y_{2,i} - y_{1,i}$ (vertical height). $\beta = 1.3$ is an empirically tuned scaling factor. The adaptive threshold \mathcal{T}_l is:

$$\mathcal{T}_l = \beta \cdot \text{median}(\{l_i\}_{i=1}^N) \quad (1)$$

Cross-layout elements are detected via two criteria: (1) $l_i > \mathcal{T}_l$, and (2) horizontal projection overlap with at least 2 other blocks. The judgment function $\mathcal{C}_{\text{cross}}(B_i)$ is defined as:

$$\mathcal{C}_{\text{cross}}(B_i) = \begin{cases} 1 & l_i > \mathcal{T}_l \wedge \sum_{j \neq i} \mathbb{I}_{\text{overlap}}(B_i, B_j) \geq 2 \\ 0 & \text{otherwise} \end{cases} \quad (2)$$

Here, $\mathbb{I}_{\text{overlap}}(B_i, B_j)$ is an indicator function (1 for horizontal projection overlap, 0 otherwise). Detected cross-layout elements are masked for subsequent layout-aware splitting, while single-layout elements (within one grid unit) are processed immediately to avoid interference.

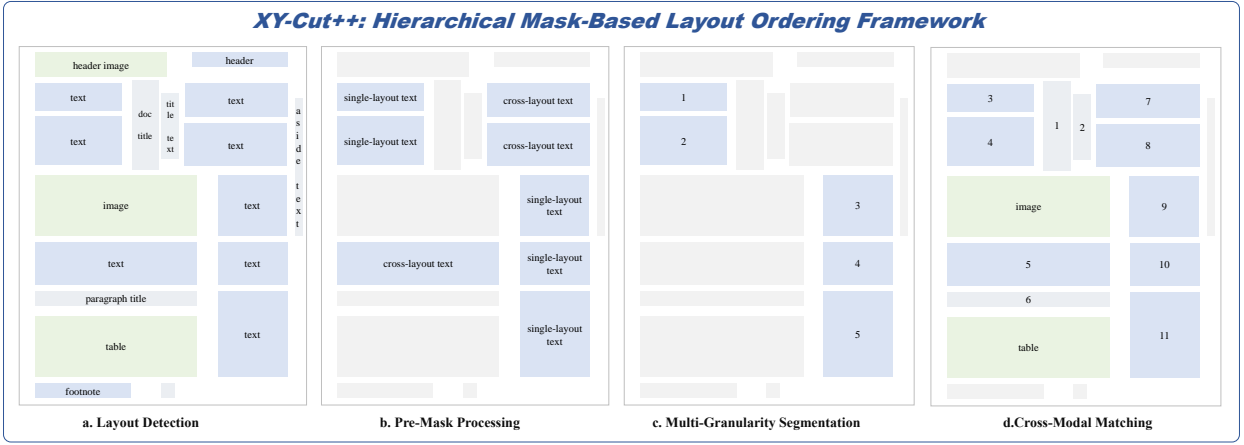


Fig. 5 End-to-End Layout Ordering for Diverse Document Layouts Framework Overview: (a) Layout Detection (PP-DocLayout [19]), (b) Pre-Mask Processing, (c) Multi-Granularity Segmentation, and (d) Cross-Modal Matching.

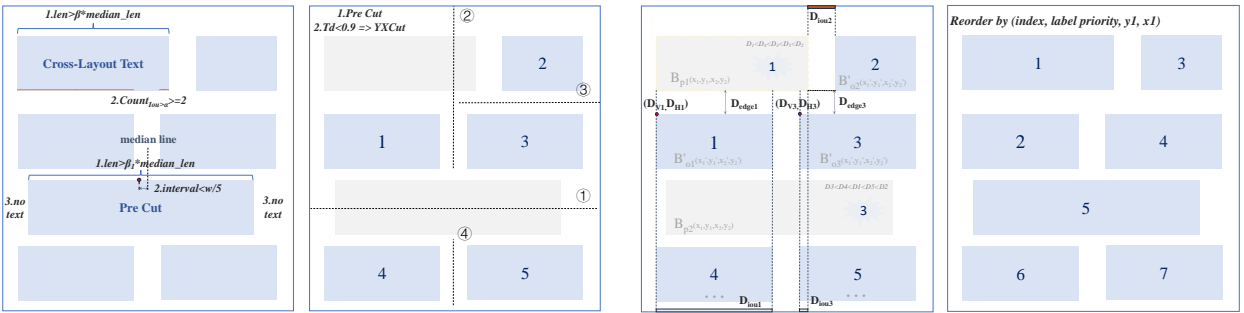


Fig. 6 Multi-Granularity Segmentation: (1) cross-layout element masking, (2) preliminary segmentation via pre-cut (①), and (3) recursive density-driven partitioning. The enhanced XY-Cut algorithm adapts its splitting axis selection through real-time density evaluation (τ_d), prioritizing horizontal splits for content-dense regions and vertical splits otherwise (②③).

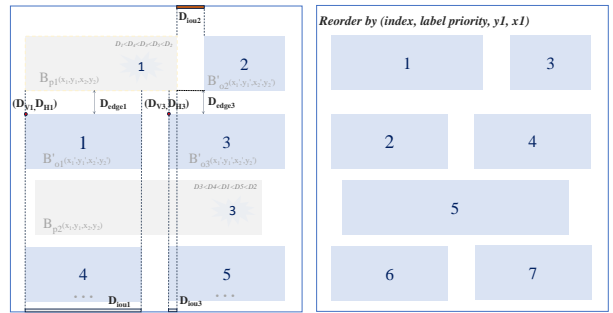


Fig. 7 Cross-Modal Matching: (1) semantic hierarchy-aware stage decomposition and (2) adaptive distance metric matching with dynamic policies and semantic-specific tuning. Subsequently, cells are reordered based on Index, Label Priority, Y1, and X1.

Phase 2: Geometric Pre-Segmentation This phase aims to identify central content elements, including body titles (e.g., chapter and section titles), and isolated graphical components (e.g., figures and tables). These elements are leveraged to perform coarse-grained partitioning of the original page into multiple non-overlapping sub-regions, denoted as R . Each R is subsequently subjected to density-driven adaptive refinement in Phase 3 to achieve fine-grained segmentation. Such elements are classified based on geometric features, formalized by the judgment function $\mathcal{P}(B_i)$:

$$\mathcal{P}(B_i) = \mathbb{I} \left(\frac{\|c_i - c_{\text{page}}\|_2}{d_{\text{page}}} \leq 0.2 \right) \wedge (\phi_{\text{text}}(B_i) = \infty), \quad (3)$$

Where:

- $c_i = (cx_i, cy_i)$: Center of B_i , computed as $cx_i = \frac{x_{1,i} + x_{2,i}}{2}$, $cy_i = \frac{y_{1,i} + y_{2,i}}{2}$;
- c_{page} : Page center coordinate;
- $\|c_i - c_{\text{page}}\|_2$: Euclidean distance between B_i and page center;
- d_{page} : The normalization factor d_{page} is determined by the block type:

$$d_{\text{page}} = \begin{cases} W_{\text{page}}, & \text{if } r_i < 3, \\ H_{\text{page}}, & \text{if } r_i \geq 3, \end{cases} \quad \text{where } r_i = \frac{w_i}{h_i} = \frac{x_{2,i} - x_{1,i}}{y_{2,i} - y_{1,i}},$$

and W_{page} , H_{page} are the page width and height, respectively.

$\mathbb{I}(\cdot)$: Indicator function (1 if condition holds, 0 otherwise);

$\phi_{\text{text}}(B_i)$: Minimum Euclidean distance from B_i to the nearest text block; $\phi_{\text{text}}(B_i) = \infty$ means B_i is isolated (no adjacent text);

Target elements B_i : Body titles (chapter/section titles), visual components (e.g., Figure, Table), all with high layout flexibility.

Elements with $\mathcal{P}(B_i) = 1$ are marked as isolated and added to the mask set. Their coordinates are used to split the page into non-overlapping sub-regions R , laying the groundwork for recursive refinement.

Phase 3: Density-Driven Refinement To achieve fine-grained segmentation, we apply the adaptive XY-Cut algorithm to each coarse-grained sub-region R from Phase 2. This algorithm dynamically selects the splitting axis (horizontal/vertical) based on regional content density of the current sub-region R . The density metric τ_d quantifies the ratio of cross-layout element area to single-layout element area within R , calculated as:

$$\tau_d = \frac{\sum_{k=1}^{N_c} w_k^{(C_c)} h_k^{(C_c)}}{\sum_{k=1}^{N_s} w_k^{(C_s)} h_k^{(C_s)}}, \quad (4)$$

where C_c and C_s are cross-layout and single-layout element sets in R ; N_c, N_s are their counts. $w_k^{(C_c)} h_k^{(C_c)}$ and $w_k^{(C_s)} h_k^{(C_s)}$ represent the area of the k -th element in each set, respectively.

A higher τ_d indicates a denser distribution of cross-layout elements (typically horizontal content). We set a density threshold $\theta_v = 0.9$ to determine the splitting direction, as defined by the strategy function $\mathcal{S}(R)$:

$$\mathcal{S}(R) = \begin{cases} \text{XY-Cut} & \tau_d > \theta_v \\ \text{YX-Cut} & \text{otherwise} \end{cases} \quad (5)$$

Here, XY-Cut refers to prioritizing horizontal splitting (along the Y-axis): we compute the Y-axis projection histogram of region R , find the position y_{cut} with the minimum projection value (i.e., the "gap" between content blocks), and split R into upper and lower sub-regions. YX-Cut prioritizes vertical splitting (along the X-axis) using the same logic on the X-axis projection histogram.

The recursive splitting process terminates when each sub-region contains only one non-masked content block. Each final atomic region R_i is represented as a 7-tuple, encapsulating spatial coordinates, content type, semantic label, and positional index:

$$R_i = \langle x_1^{(i)}, y_1^{(i)}, x_2^{(i)}, y_2^{(i)}, C_i, \text{Label}_i, \text{Index}_i \rangle \quad (6)$$

where $(x_1^{(i)}, y_1^{(i)})$ and $(x_2^{(i)}, y_2^{(i)})$ denote the top-left and bottom-right coordinates of R_i ; $C_{\text{type}} = \{\text{cross-layout}, \text{single-layout}\}$, with $C_i \in C_{\text{type}}$ indicating the content type of R_i ; Label_i represents the semantic label (e.g., title, figure, paragraph) of R_i ; and Index_i denotes the positional index of R_i in the document layout. This 7-tuple representation provides comprehensive information to support subsequent cross-modal matching.

4.3 Cross-Modal Matching

To establish reading coherence consistent with human habits, we propose a geometry-aware cross-modal alignment framework, consisting of multi-stage semantic filtering and adaptive distance metric modules (Figure 7). This framework fuses semantic priority and geometric constraints to realize accurate ordering of atomic regions.

Multi-Stage Semantic Filtering: This module realizes the restoration of masked elements and optimizes the ordering sequence by leveraging label priority, ensuring high-semantic elements (e.g., cross-layout text, titles) are prioritized in the matching and restoration process. We first define core sets and a global label priority sequence, then formalize the matching logic to sequentially restore masked elements into the ordered sequence.

The multi-stage semantic filtering module restores masked elements by leveraging a global label priority sequence $\mathcal{L}_{\text{order}}$. The process operates on three core sets: the pre-ordered atomic region set S , the masked element set \mathcal{M} , and the dynamically updated target sequence T (initialized as $T = S$). The mathematical formulation is:

$$\begin{aligned} \mathcal{L}_{\text{order}} &: \mathcal{L}_{\text{cross-layout}} \succ \mathcal{L}_{\text{title}} \succ \mathcal{L}_{\text{vision}} \succ \mathcal{L}_{\text{others}} \\ \mathcal{F}(B_p, T, l_{\text{current}}) &= \begin{cases} 1, & \exists B_o \in T, \mathcal{L}_{\text{order}}(l(B_o)) \succ \mathcal{L}_{\text{order}}(l_{\text{current}}) \\ 0, & \text{otherwise} \end{cases} \\ \mathcal{M}^{(l_{\text{current}})}_{\text{sorted}} &= \{(B_p, B_{\text{best}}) \mid B_p \in \mathcal{M}, l(B_p) = l_{\text{current}}, \mathcal{F} = 1, B_{\text{best}} \in T\} \\ T &= T \cup \mathcal{M}^{(l_{\text{current}})}_{\text{sorted}}, \quad \forall l_{\text{current}} \in \mathcal{L}_{\text{order}} \end{aligned} \quad (7)$$

Here, the binary matching function \mathcal{F} verifies for a pending element B_p (with label l_{current}) whether a higher-priority candidate exists in T . For each B_p that satisfies $\mathcal{F} = 1$, the specific optimal anchor $B_{\text{best}} \in T$ is determined by minimizing a joint geometric distance (detailed in the following Adaptive Distance Metric).

The set $\mathcal{M}_{\text{sorted}}^{(l_{\text{current}})}$ then contains all such matched pairs (B_p, B_{best}) for the current label. These pairs are subsequently integrated into T , and the process iterates through $\mathcal{L}_{\text{order}}$, ensuring high-priority elements are restored first.

This multi-stage semantic filtering strategy effectively eliminates irrational matching pairs (e.g., visual elements paired with footnotes) and reinforces the semantic coherence of the final ordered sequence, laying a solid foundation for downstream cross-modal alignment.

Adaptive Distance Metric: We design a joint geometric distance metric with early termination to find the optimal matching position for each B_p in \mathcal{M}_{sem} . Given a pending layout element $B_p = (x_1, y_1, x_2, y_2)$ and an ordered candidate $B_o = (x'_1, y'_1, x'_2, y'_2)$, the distance $D(B_p, B_o, l)$ (parameterized by B_p 's label l) is a weighted sum of four geometric constraints ϕ_k :

$$D(B_p, B_o, l) = \sum_{k=1}^4 w_k \cdot \phi_k(B_p, B_o), \quad (8)$$

where w_k are adaptive weights (detailed later), and $\phi_1 \sim \phi_4$ encode different geometric constraints to capture spatial relationships:

- *Intersection Constraints (ϕ_1): Filters invalid pairs by layout direction and overlap. The overlap threshold is set to $\tau_{\text{overlap}} = 0.3$.*

$$\phi_1 = \begin{cases} 1, & \text{if } \text{direction}(B_p) \neq \text{direction}(B'_o) \vee \text{IoU}_{\text{projection}} < \tau_{\text{overlap}} \\ 0, & \text{otherwise} \end{cases} \quad (9)$$

- *Boundary Proximity (ϕ_2): Measures spatial adjacency. Weighted by w_{edge} , it uses center distances, prioritizing axis-aligned adjacency.*

$$\phi_2 = w_{\text{edge}} \times \begin{cases} d_x + d_y, & \text{(diagonal adjacency)} \\ \min(d_x, d_y), & \text{(axis-aligned)} \end{cases} \quad (10)$$

- *Vertical Continuity (ϕ_3): Optimizes vertical ordering.*

$$\phi_3 = \begin{cases} -y'_2, & l \in \mathcal{L}_{\text{cross-layout}} \wedge y_1 > y'_2 \\ y'_1, & \text{(baseline alignment)} \end{cases} \quad (11)$$

- *Horizontal Ordering (ϕ_4): Follows left-to-right reading logic via B_o left boundary.*

$$\phi_4 = x'_1 \quad (12)$$

We introduce two parameterization strategies to optimize the metric's adaptability:

Dynamic Weight Adaptation. To ensure the four geometric constraint distances do not interfere with each other, we design scale-sensitive weights with staggered scaling levels. The weight vector $\mathbf{w}_k = [w_1, w_2, w_3, w_4]$ is formulated as:

$$\mathbf{w}_k = [\max(h, w)^2, \max(h, w), 1, \max(h, w)^{-1}] \quad (13)$$

where h, w denote page dimensions, it establishes a distance metric with clear priorities.

Semantic-Specific Tuning. Optimal weights from grid search on 2.8k documents:

$$\mathbf{w}_{\text{edge}} = \begin{cases} [1, 0.1, 0.1, 1] & l \in \mathcal{L}_{\text{title}} \cap \mathcal{O}_{\text{horizontal}} \\ [0.2, 0.1, 1, 1] & l \in \mathcal{L}_{\text{title}} \cap \mathcal{O}_{\text{vertical}} \\ [1, 1, 0.1, 1] & l \in \mathcal{L}_{\text{cross-layout}} \\ [1, 1, 1, 0.1] & l \in \mathcal{L}_{\text{otherwise}} \end{cases} \quad (14)$$

where $\mathcal{O}_{\text{horizontal}}$ and $\mathcal{O}_{\text{vertical}}$ denote the horizontal layout set and vertical layout set, respectively; l is the semantic label of the element. This weight design assigns differentiated weights based on label characteristics and layout orientations, further weakening mutual interference between constraints and improving matching stability across various scenarios.

Statistical validation demonstrates significant improvements: +2.3 BLEU-4 over uniform baselines. The overall process can be simply expressed in Algorithm 1.



Fig. 8 Visualization of Complex Page D_c from DocBench-100 Dataset Using Different Layout Analysis Methods. (a) Input Image, (b) XY-Cut [1], classic projection-based segmentation, (c) MinerU [20], an end-to-end Document Content Extraction tool, (d) XY-Cut++, our proposed method.

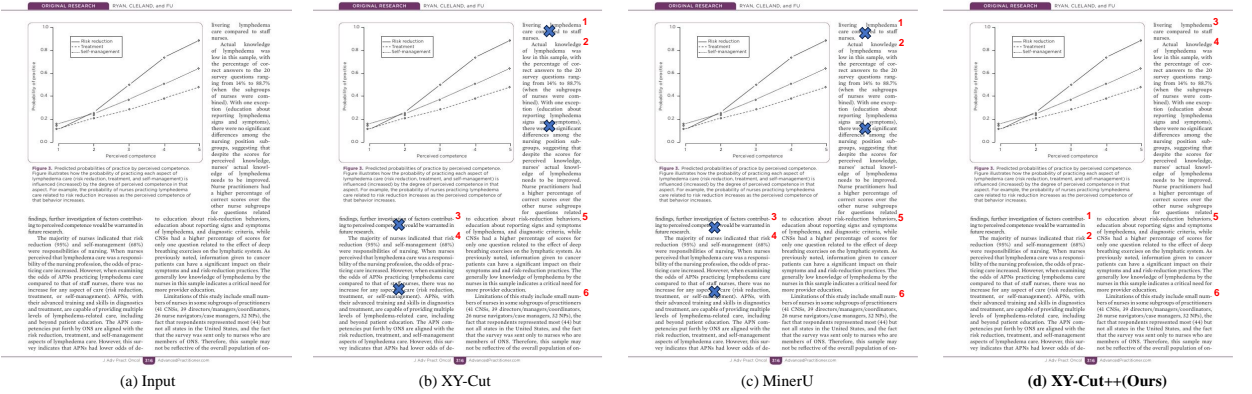


Fig. 9 Visualization of Regular Page D_r from DocBench-100 Dataset Using Different Layout Analysis Methods. (a) Input Image, (b) XY-Cut [1], a classic projection-based segmentation, (c) MinerU [20], an end-to-end Document Content Extraction tool, (d) XY-Cut++, our proposed method.

Table 2 Progressive Component Analysis on DocBench-100. *Metric Key:* BLEU-4 \uparrow / ARD \downarrow / Tau \uparrow .

Method	D_c			D_r			μ		
	BLEU-4	ARD	Tau	BLEU-4	ARD	Tau	BLEU-4	ARD	Tau
XY-Cut	0.749	0.233	0.878	0.819	0.098	0.912	0.797	0.139	0.902
+Pre-Mask	0.818	0.196	0.887	0.823	0.087	0.920	0.822	0.120	0.910
+MGS	0.946	0.164	0.969	0.969	0.036	0.985	0.962	0.074	0.980
+CMM	0.986	0.023	0.995	0.989	0.003	0.997	0.988	0.009	0.996

5 Experiments

In this section, we describe the experimental setup for evaluating our proposed method on the DocBench-100 benchmark. We compare our approach with several state-of-the-art baselines and demonstrate its effectiveness through both quantitative and qualitative analyses.

5.1 Dataset

We evaluate on DocBench-100; detailed sources, fields, annotation pipeline, screening criteria, statistics, and usage protocols are described in Section 3. For fairness, we report both end-to-end and JSON-based protocols, and clarify FPS timing scope alongside Table 6.

5.2 Setup

Baselines

We compare our method with the following state-of-the-art approaches:

- **XY-Cut [1]:** A classic method for projection-based segmentation.

Algorithm 1 Geometry-Aware Cross-Modal Matching with Semantic Filtering

Require: Sorted anchor set \mathcal{S} , masked element set \mathcal{M} , distance weights w_1, w_2, w_3, w_4 **Ensure:** Matching result set \mathcal{T}

```
1: Initialize global label priority:  $\mathcal{L}_{\text{order}} : \mathcal{L}_{\text{cross-layout}} \succ \mathcal{L}_{\text{title}} \succ \mathcal{L}_{\text{vision}} \succ \mathcal{L}_{\text{other}}$ 
2:  $\mathcal{T} \leftarrow \{(B_o, B_p) \mid B_o \in \mathcal{S}\}$  ▷ Initialize with self-pairs of anchors
3: for each semantic label  $l$  in  $\mathcal{L}_{\text{order}}$  (descending priority) do
4:   for each pending box  $B_p \in \mathcal{M}$  with label  $l$  do ▷ Check  $\mathcal{F}(B_p, \mathcal{T}, l)$ 
5:      $D_{\min} \leftarrow \infty, B_{\text{best}} \leftarrow \text{null}$ 
6:     for each ordered box  $B_o$  in  $\mathcal{T}$  do ▷ Search candidates in  $\mathcal{T}$  for  $\mathcal{F}$ 
7:        $D_{\text{curr}} \leftarrow 0$ 
8:       for  $k \leftarrow 1$  to 4 do
9:          $D_{\text{curr}} \leftarrow D_{\text{curr}} + w_k \cdot \phi_k(B_p, B_o)$ 
10:        if  $D_{\text{curr}} > D_{\min}$  then
11:          break ▷ Early termination
12:        end if
13:      end for
14:      if  $D_{\text{curr}} < D_{\min}$  then
15:         $D_{\min} \leftarrow D_{\text{curr}}, B_{\text{best}} \leftarrow B_o$ 
16:      end if
17:    end for
18:    if  $B_{\text{best}} \neq \text{null}$  then ▷ Valid match found for  $B_p$ 
19:       $\mathcal{T} \leftarrow \mathcal{T} \cup \{(B_p, B_{\text{best}})\}$  ▷  $\mathcal{M}_{\text{sorted}}^{(l)} \leftarrow \mathcal{M}_{\text{sorted}}^{(l)} \cup \{(B_p, B_{\text{best}})\}$ 
20:    end if
21:  end for
22:  Sort  $\mathcal{T}$  by: Label priority of  $B_p$  (desc)  $\succ$  Index of  $B_{\text{best}}$  (asc)  $\succ$   $y_1$  of  $B_p$  (asc)  $\succ$   $x_1$  of  $B_p$  (asc)
23: end for
24: return  $\mathcal{T}$ 
```

Table 3 Ablation Study of Pre-Mask, Multi-Granularity Segmentation (MGS), and Cross-Modal Matching (CMM) on DocBench-100. *Metric Key:* BLEU-4 \uparrow .

Method	Mask	Mask Cross-Layout	Pre-Cut	Adaptive Scheme	ϕ_1	ϕ_2	ϕ_3	ϕ_4	Dynamic Weights	Multi-Stage	BLEU-4
Baseline											0.797
+Pre-Mask	✓										0.822
+MGS	✓	✓									0.905
	✓		✓								0.914
	✓			✓							0.923
	✓	✓	✓	✓							0.962
+CMM	✓	✓	✓	✓						✓	0.963
	✓	✓	✓	✓	✓					✓	0.765
	✓	✓	✓	✓		✓				✓	0.858
	✓	✓	✓	✓			✓		✓	✓	0.985
	✓	✓	✓	✓				✓		✓	0.881
	✓	✓	✓	✓					✓	✓	0.694
	✓	✓	✓	✓	✓	✓	✓	✓	✓	✓	0.988

- **LayoutReader** [2, 10]: A LayoutLMv3-based model fine-tuned on 500k samples.
- **MinerU** [20]: An end-to-end document content extraction tool.

Evaluation Metrics

We evaluate the performance using the following metrics:

- **BLEU-4** [21] (\uparrow): Measures the similarity between candidate and reference texts using up to 4-gram overlap.
- **ARD** (\downarrow): Absolute Relative Difference, quantifies prediction accuracy by comparing predicted and actual values.
- **Tau** (\uparrow): Kendall’s Tau, measures the rank correlation between two sets of data.
- **FPS** (\uparrow): Frames Per Second, a measure of how many frames a system can process per second.

Block-level BLEU (detection order). We evaluate the ordering of *detection boxes* (block IDs), not textual content. Following the original BLEU definition [21], we compute n-gram precisions on block identifiers

Table 4 Reading Order Recovery Performance: BLEU-4 \uparrow Results on DocBench-100. The best results are in bold.

Method	D_c	D_r	μ
XY-Cut [1]	0.749	0.818	0.797
LayoutReader [2, 10]	0.656	0.844	0.788
MinerU [20]	0.701	0.946	0.873
XY-Cut++(ours)	0.986	0.989	0.988

Table 5 Reading Order Recovery Performance on Textual Content of OmniDocBench (Excluding Figures/Tables with Insignificant Layout Impact). *Metric Key:* BLEU-4 \uparrow / ARD \downarrow / Tau \uparrow . Best results are in **bold**; second-best are underlined.

Method	Single			Double			Three			Complex			Mean		
	BLEU-4	ARD	Tau												
XY-Cut [1]	0.895	0.042	0.931	0.695	0.230	0.794	0.702	0.090	0.923	0.717	0.120	0.866	0.753	0.118	0.878
LayoutReader [2, 10]	<u>0.988</u>	0.004	<u>0.995</u>	0.831	0.084	0.918	0.595	0.208	0.805	0.716	0.116	0.864	0.783	0.099	0.906
MinerU [20]	0.961	<u>0.025</u>	0.969	<u>0.933</u>	<u>0.037</u>	<u>0.971</u>	<u>0.923</u>	<u>0.042</u>	<u>0.965</u>	<u>0.887</u>	0.050	<u>0.932</u>	<u>0.926</u>	<u>0.039</u>	<u>0.959</u>
XY-Cut++(ours)	0.993	0.004	0.996	0.951	0.027	0.974	0.967	0.033	0.984	0.901	<u>0.064</u>	0.942	0.953	0.037	0.972

Table 6 Model Efficiency and Semantic Information Usage on DocBench-100 and OmniDocBench. *Key Metrics:* FPS (Total Pages/Total Times) \uparrow . FPS values are averaged over 10 runs on Intel(R) Xeon(R) Gold 6326 CPU @ 2.90GHz with 256GB memory. Best results are in **bold**; second-best are underlined.

Method	Semantic Info	FPS		
		DocBench-100	OmniDocBench	Mean
XY-Cut [1]	X	<u>685</u>	289	<u>487</u>
LayoutReader [2, 10]	X	17	27	22
MinerU [20]	X	10	12	11
XY-Cut++(ours)	✓	781	<u>248</u>	514

and report BLEU-4 *with* brevity penalty:

$$\text{BLEU}_4(\hat{s}, s) = BP \cdot \exp \left(\sum_{n=1}^4 \frac{1}{4} \log p_n \right), \quad (15)$$

where p_n is the precision of block-level n-grams and $BP = \begin{cases} \exp(1 - r/c), & c \leq r \\ 1, & c > r \end{cases}$ with c the hypothesis length and r the reference length.

FPS measurement scope. Table 6 reports FPS for the ordering/sorting module only; upstream detection (e.g., PP-DocLayout) and downstream OCR/LM are excluded. Results are averaged over 10 runs on Intel(R) Xeon(R) Gold 6326 CPU @ 2.90GHz, 256GB RAM.

5.3 Main Results

We evaluate our method on DocBench-100, analyzing component contributions and comparing against state-of-the-art baselines. All metrics are computed over the union of D_c and D_r , subsets unless specified.

5.3.1 Progressive Component Ablation

Table 2 demonstrates the cumulative impact of each technical component:

- **XY-Cut Baseline:** Achieves 0.749 BLEU-4 on complex layouts (D_c), showing limitations in handling complex layouts (e.g., L-shaped) elements.
- **+Pre-Mask:** Improves BLEU-4 by 6.9 points (from 0.749 to 0.818) on D_c via adaptive thresholding (Eq. (1), $\beta = 1.3$), reducing false splits by 15.9%.
- **+MGS:** Delivers a 19.7 absolute BLEU-4 gain on D_c through three-phase segmentation, with density-aware splitting (Eq. (5)) reducing ARD by 29.7%.
- **+CMM:** Achieves near-perfect alignment (0.995 τ) on D_c through geometric constraints (Eq. (9)–(12)), finalizing a 90.1% ARD reduction from baseline.

The complete model reduces ARD by 93.5% compared to baseline ($0.139 \rightarrow 0.009$), demonstrating superior ranking consistency. Notably, our method maintains balanced performance across both subsets ($0.988 \mu\text{-BLEU}$), proving effective for diverse layout types.

5.3.2 Architectural Analysis

We perform a systematic dissection of core components through controlled ablations to evaluate their contributions:

Pre-Mask Processing (Pre-Mask): To alleviate the "L-shaped" problem, we applied preliminary masking on highly dynamic elements such as titles, tables, and figures (see Methods Section 4.1). This approach reduced visual noise and improved reading order recovery, resulting in a 2.5-point BLEU-4 score increase, as shown in Table 3.

Multi-Granularity Segmentation (MGS): Mask cross-layout is a very direct method to solve the problem that XY-Cut cannot segment L-shaped input. Pre-Cut realizes preliminary sub-page division through page analysis, thereby avoiding page content mixing affecting sorting. The adaptive splitting strategy enables reasonable segmentation through real-time density estimation. Table 3 shows additive benefits of the mask cross-layout (+8.3), Pre-Cut (+9.2), and the adaptive splitting scheme (+10.1) over the baseline (0.822 BLEU-4).

Cross-Modal Matching (CMM): As shown in Table 3, the single-stage strategy performs comparably to the baseline approach. This suggests that employing a detection model equipped with text, title, and annotation labels is sufficient to achieve nearly consistent performance across various scenarios. Notably, on the OmniDocBench dataset, which has few label categories, our method still achieves state-of-the-art results. Furthermore, we observe that the edge-weighted margin distance plays a crucial role among the four distance metrics examined. This finding highlights the significance of dynamic weights based on shallow semantics. In contrast, implementing cross-modal matching results in an overall improvement of 2.7 points in BLEU-4 scores.

5.3.3 Benchmark Comparison

As shown in Table 4, our approach establishes new benchmarks across all evaluation dimensions. Specifically, it outperforms XY-Cut by a significant margin, achieving a +23.7 absolute improvement on D_c (from 74.9 to 98.6). Additionally, it surpasses LayoutReader by +5.3 on D_r (from 94.6 to 98.9), despite not using any learning-based components. Furthermore, our method achieves a Kendall’s τ of 0.996 overall, indicating near-perfect ordinal consistency (with $p < 0.001$ in the Wilcoxon signed-rank test). Visual results presented in Figure 8 and 9 further demonstrate the robustness in handling multi-column layouts and cross-page elements, where previous methods frequently fail.

To further validate the versatility and robustness of our proposed method, we conducted extensive evaluations on the OmniDocBench dataset [3], which features a diverse and challenging set of document images. As shown in Table 5, our proposed method (XY-Cut++) achieves state-of-the-art (SOTA) performance across almost all layout types, despite challenging subpage nesting patterns (see Limitations). Notably, as shown in Table 6, XY-Cut++ achieves a superior balance between performance and speed, attaining an average FPS of 514 across DocBench-100 and OmniDocBench. This performance surpasses even the direct projection-based XY-Cut algorithm, which achieves an average FPS of 487. The significant speed improvement of XY-Cut++ is primarily attributed to semantic filtering, which minimizes redundant processing by handling each block only once. In contrast, XY-Cut requires repeatedly partitioning blocks into different subsets, resulting in increased recursive depth and computational overhead. This optimization enhances computational efficiency without losing performance, making XY-Cut++ more robust and versatile for diverse document layouts.

6 Discussion

XY-Cut++ closes the gap between classical projection-based methods and neural models for block-level reading-order recovery through a simple three-stage pipeline. Directional ordering (left-to-right, top-to-bottom) is largely solved; the remaining pain points are fine-grained semantic segmentation (e.g., ambiguous block boundaries and caption linkage; see Figure A8) and sub-page structures. Across DocBench-100 and OmniDocBench, XY-Cut++ delivers large, consistent gains (Table 2, Table 5) while retaining high throughput on CPU (Table 6). On D_c , BLEU-4 rises from 0.749 to 0.986 and ARD falls from 0.233 to 0.023, with visual results (Figures 8,9) confirming robustness on multi-column and L-shaped cases.

Mechanistically, the three components are complementary: Pre-Mask suppresses dominant elements to expose a stable backbone; MGS uses an adaptive density τ_d (Eq. (4)) to choose the split axis (Eq. (5)); and

CMM applies four geometric constraints (Eqs. (9)–(12)) with scale-aware (Eq. (13)) and semantic-specific weights (Eq. 14). Ablations indicate edge-weighted margins are especially effective.

Practically, reliable block-level ordering benefits RAG/LLM preprocessing by improving chunking and caption attachment, and XY-Cut++ is easy to deploy after a detector with coarse labels (e.g., PP-DocLayout). DocBench-100 helps standardize block-level evaluation and emphasizes difficult page topologies.

Limitations primarily stem from label granularity for fine-grained segmentation and from nested “sub-pages” (Figure A8); detector quality also matters. Heuristic hyperparameters (e.g., β in Eq. (1), θ_v in Eq. (5)) may require domain tuning. Future work targets: (i) sub-page detection with hierarchical reasoning to localize ordering, (ii) learning the split policy and edge weights from weak supervision to improve within-block segmentation, and (iii) coupling lightweight language priors (caption/title cues) with end-to-end RAG/LLM evaluation.

7 Conclusion

We studied block-level reading-order recovery for real-world documents, a prerequisite for reliable RAG/LLM pipelines. We proposed XY-Cut++, a hierarchical, geometry-aware framework that integrates pre-mask processing, multi-granularity segmentation, and cross-modal matching. XY-Cut++ delivers precise block ordering and achieves state-of-the-art performance on DocBench-100 and OmniDocBench, while maintaining high throughput on CPU (cf. Tables 2, 6).

This accuracy–efficiency balance is achieved via two design choices: (i) shallow semantic labels used as structural priors and (ii) a hierarchical mask mechanism that stabilizes XY-Cut through density-aware splitting and edge-weighted matching. These components jointly improve accuracy without sacrificing throughput, making XY-Cut++ a practical module for production-grade document parsing. Beyond the algorithm, DocBench-100 offers a focused, block-level benchmark that emphasizes challenging page topologies and promotes standardized evaluation. Future work will extend XY-Cut++ with sub-page detection and lightweight language priors to better handle nested and fine-grained structures (see Section 6).

Appendix A Additional Visual Results

A.1 Other Cases



Fig. A1 DocBench-100 (complex subset) — Example A. A challenging multi-column page with spanning titles and interleaved elements. XY-Cut++ maintains a coherent block-level reading order across columns by combining pre-mask and density-aware splitting.



Fig. A2 DocBench-100 (complex subset) — Example B. Nested regions and interleaved figures/captions. The mask-then-remap strategy reduces L-shape artifacts and preserves local grouping for globally consistent ordering.

带薪休病假、特许爱人带薪陪同、定期安排复检……工人代春霞——

“公司像关爱亲人一样呵护员工”

本报记者 邵玉梁

就业故事·携手渡难关

一条流水线上传来一片橡胶鞋底，代春霞抓起其中一块仔细察看，检查合格后放回传送带传递给工友打包入库……车间组长郭文水从她身旁走过，又开始叮嘱：“小代，累了就坐下歇会儿。身体第一位！”代春霞笑着摆摆手：“没事儿，这才站了多长时间呢！不累！”

今年43岁的代春霞是福建省泉州市某轻工公司橡胶车间的一名工人。自2009年入职以来，她和爱人王晓伟已经在这个车间一同工作了11年。“你问为啥能在这干这么久？对我们好啊，公司像关爱亲人一样呵护员工！”代春霞说。

去年7月，代春霞确诊乳腺癌。为鼓励她积极治疗，公司不仅让她本人带薪治病，还特许她的爱人带薪陪同治疗。“没有公司的大力支持，我不会康复这么快！”代春霞说。今年3月初，代春霞痊愈后返岗，公司为她安排了新岗位的同时，还贴心地送上了大礼包：一次性现金补助、定期身体复检……“我回到公司，感觉跟到家一样。”代春霞说，“我们要在这一干到退休！”

“安安心心回去把病治好！”

“多亏体检及时发现，不然癌细胞扩散了可就麻烦了。”回想起去年患病治疗的经历，代春霞至今深感幸运。“公司一直特别关注我们员工的健康问题，每年体检、义诊、健康讲座，一样不少，专门建了运动广场不说，还和两家定点医院合作，方便我们随时就医。”

去年7月，公司如期组织全体职工体检。和往常一样，体检报告下发个人时，工会主席黎益群总不忘再三叮嘱有问题及时应

核心阅读

橡胶车间工人代春霞，去年确诊乳腺癌，公司给予了多种帮助：让她带薪休病假，特许她同在公司上班的爱人带薪陪同照顾，直到代春霞病情基本痊愈，才安排她返回公司上班，还给了现金补助。返岗后，密切关注她的身心健康状况，多加照顾，安排复检，让代春霞感到温暖。代春霞并不是个案，特别是疫情防控以来，企业正在采取多种措施关爱员工，切实保障员工身心健康。

。看到自己的体检报告上赫然写着“乳腺肿块”，再加上身体不时有不舒适，代春霞心里没底，便将信息反馈给了车间主任。“明天你去区医院再好好查查，费用公司出。”不到一小时，代春霞就接到了黎益群的电话，告知她公司已为她预约好了第二天的复查。

“医生说彩超显示乳腺肿块有4a级，建议我做钼靶。”检查结果一出来，代春霞便及时告诉了黎益群。“行，但区医院毕竟条件有限，还是去市医院查吧！”

泉州180医院的专家一看，建议直接手术治疗。“你这肿块不小，必须切除化验。”代春霞是河南人，在老家襄城县上了新农保。来公

司上班以后，公司又给出了工伤保险、意外险，还参与了泉州市职工医疗互助活动。治疗有报销，可仍是一笔大支出，怎样最划算呢？代春霞算不明白，又请教了黎益群。

“在泉州动手术，属异地医疗，医保只能报到40%，回老家襄城，能报到70%。”黎益群说。代春霞和爱人一合计，决定请半个月的假回家动手术，报销比例高不说，还有家人在身边悉心照顾。

“你别管请假多久，先安安心心回去把病治好！”得知代春霞的决心，黎益群立即帮她订好第二天的机票，并派了专车送机。

“当时上网查，说大部分都是良性肿块，切了就没事。恶性的概率特别小！”代春霞一开始很乐观，可是公司却不放心。“治疗期间，我每天给你补贴90元。什么时候医生说没问题了，再回来好好上班。”送机路上，黎益群仍不停叮嘱。

“公司永远是你们的大后方！”

2019年7月28日，代春霞在襄城县医院进行了切除手术。肿块化验结果显示为恶性。“一下子紫了！怎么可能呢？”她想不通，明明是极小的概率，为什么却还是落在了自己的头上。

在千里之外的泉州，得知爱人确诊消息后的王晓伟也一下子蔫了。一直挂心的黎益群赶忙向董事长郭修彬做了紧急汇报。“马上帮小王订票，让他带薪休假回去陪同小代治疗。”黎益群马上帮王晓伟订下最近的航班机票。“你回去的任务就是照顾好你爱人。有什么问题时联系，公司永远是你们的大后方。”出发前，黎益群同王晓伟交代。

第二天一早，看到爱人出现在病房，代春霞哭了。“他来了，我心里就踏实了。”代春霞说，公司不

仅每天关心她的身体和心理状态，还关注丈夫的心理状况，每晚都会通过电话交流。“我必须尽快振作起来，好好接受治疗，争取早点康复，回去上班。”代春霞暗暗下了决心。

“幸亏发现得早，癌细胞没有扩散，后期配合化疗，问题不大。”手术后的第四天，当医生告知最终化验结果时，夫妻俩悬着的心终于放下来。快一个月的时候，代春霞获准出院。想着家人可以轮流照顾自己，她想让王晓伟先回公司上班，公司却不同意。“不行，先等她身体养好再回来。只要身体没问题，你们随时回来，随时欢迎！”黎益群对王晓伟说。

在王晓伟的精心照顾下，代春霞顺利通过了复查，可以开始化疗。“我现在生活能自理了，心态也很好，而且化疗有姐姐陪，真的不用担心。”在代春霞的坚持下，王晓伟又向公司递交了返岗申请。这回，公司终于同意了。

“我回来以后，黎主席每天都会跑到车间问问情况。”而远在河南的代春霞，则是每次化疗前必会接到公司打来的慰问电话，“领导叮嘱我照顾好身体，担心我害怕化疗，鼓励我积极面对。”今年2月，代春霞第八次化疗完成，再次回到医院复查，终于收获了“基本痊愈”的好消息。

“员工返岗支持公司，我们必须对他们的健康负责！”

春节过后，受疫情影响，公司没有开工。到了3月，迎来复工的消息，“我们最困难的时候是公司一直在支持，现在公司需要我们，我们必须去！”3月初，夫妻俩搭乘工友的顺风车一同返岗。

“终于回家了！”车刚到厂门口，代春霞便看到黎益群和几个车

间主任已在入口处等待。车辆消毒、发放防护物资、安排住宿隔离……“特殊时期，员工返岗支持公司，我们必须对他们的健康负责！”除了保障防护物资供应，提供营养餐饮服务，隔离期间公司还为每人每天发放50元的现金补助。

14天隔离期结束，考虑到代春霞的身体情况，公司为她安排了一个新岗位，代春霞从一名橡胶修边工，变成了一名品检员。“以前修边很辛苦，现在相对轻松多了，每个月工资能有六七千呢。”代春霞说。

返回岗位的第一个月，作为庆祝，公司还直接送她现金补助1.5万元。“看病一共花了12万多，新农保报销了7万多，公司补助了这么多，还通过职工互助医疗活动为我申请了5000元的大病补助，算下来自己也花了不到3万元。”代春霞算了一笔账。

“现在上班很放松，也很开心。”代春霞到了新岗位，黎益群特意嘱咐车间组长郭文水要多照顾多留心。一开始，郭文水很紧张，每过一会儿就要跑去代春霞的工位上看看有没有什么异样。几天观察下来，郭文水也放心了，“小代状态特别好。前两天我们有个工友心情不好，还是她给开导的呢！”

返岗4个多月，代春霞比以前更热爱自己的工作。“到新岗位以后，董事长还来我们车间看了我两次，问我身体恢复情况，叮嘱我有困难及时说。”今年5月，代春霞第一次愈后复查，公司不仅提前和定点医院预约好，还特许王晓伟带薪陪同复查。下个月，代春霞马上迎来第二次复查，公司也早早进行了安排。“公司让我每次复查都陪着！”王晓伟笑着说。

“身体上有不舒服、生活上有困难都要及时跟公司说，公司会尽力去解决。你们好，公司才会好！”这是董事长郭修彬经常挂在嘴边的一句话。“公司好，我们才更好。”代春霞则这样说。

Fig. A4 DocBench-100 (complex subset) — Example D. Newspaper-like dense columns. The adaptive axis selection (horizontal vs. vertical) driven by regional density yields stable column-wise ordering.



$\vec{u} = \dot{u}_r \mathbf{e}_1 + \dot{u}_\theta \mathbf{e}_2 + \dot{u}_\phi \mathbf{e}_3$ 1

so that 2

$$\frac{\partial \vec{u}}{\partial t} = \frac{\partial \dot{u}_r}{\partial t} \mathbf{e}_1 + \frac{\partial \dot{u}_\theta}{\partial t} \mathbf{e}_2 + \frac{\partial \dot{u}_\phi}{\partial t} \mathbf{e}_3$$

$$\frac{\partial \vec{u}}{\partial r} = \frac{\partial \dot{u}_r}{\partial r} \mathbf{e}_1 + \frac{\partial \dot{u}_\theta}{\partial r} \mathbf{e}_2 + \frac{\partial \dot{u}_\phi}{\partial r} \mathbf{e}_3$$

$$\frac{\partial \vec{u}}{\partial \theta} = \frac{\partial \dot{u}_r}{\partial \theta} \mathbf{e}_1 + \frac{\partial \dot{u}_\theta}{\partial \theta} \mathbf{e}_2 + \frac{\partial \dot{u}_\phi}{\partial \theta} \mathbf{e}_3$$

We know that 4

$$\frac{\partial \mathbf{e}_1}{\partial \theta} = (-\sin \theta, \cos \theta, 0) = \mathbf{e}_3, \quad \text{and} \quad \frac{\partial \mathbf{e}_3}{\partial \theta} = (-\cos \theta, -\sin \theta, 0) = -\mathbf{e}_1$$

so that 6

$$\frac{1}{r} \frac{\partial \vec{u}}{\partial \theta} = \frac{1}{r} \left(\frac{\partial \dot{u}_r}{\partial \theta} - \dot{u}_\theta \right) \mathbf{e}_1 + \frac{1}{r} \frac{\partial \dot{u}_\theta}{\partial \theta} \mathbf{e}_2 + \frac{1}{r} \left(\frac{\partial \dot{u}_\phi}{\partial \theta} + \dot{u}_r \right) \mathbf{e}_3$$

and thus 8

$$\frac{\partial \dot{u}_\alpha}{\partial \dot{u}_\beta} = \begin{pmatrix} \frac{\partial \dot{u}_r}{\partial \dot{u}_r} & \frac{\partial \dot{u}_r}{\partial \dot{u}_\theta} & \frac{\partial \dot{u}_r}{\partial \dot{u}_\phi} \\ \frac{\partial \dot{u}_\theta}{\partial \dot{u}_r} & \frac{\partial \dot{u}_\theta}{\partial \dot{u}_\theta} & \frac{\partial \dot{u}_\theta}{\partial \dot{u}_\phi} \\ \frac{\partial \dot{u}_\phi}{\partial \dot{u}_r} & \frac{\partial \dot{u}_\phi}{\partial \dot{u}_\theta} & \frac{\partial \dot{u}_\phi}{\partial \dot{u}_\phi} \end{pmatrix} \begin{pmatrix} (1/r)(\partial \dot{u}_r / \partial \theta - \dot{u}_\theta) \\ (1/r) \partial \dot{u}_\theta / \partial \theta \\ (1/r)(\partial \dot{u}_\phi / \partial \theta + \dot{u}_r) \end{pmatrix}$$

The components of the strain rate are thus 10

$$\dot{\varepsilon}_{rr} = \frac{\partial \dot{u}_r}{\partial r}, \quad \dot{\varepsilon}_{\theta\theta} = \frac{\partial \dot{u}_\theta}{\partial \theta}, \quad \dot{\varepsilon}_{\phi\phi} = \frac{1}{r} \left(\frac{\partial \dot{u}_\phi}{\partial \theta} + \dot{u}_r \right)$$

$$\dot{\gamma}_{r\theta} = 2\dot{\varepsilon}_{r\theta} = 2\dot{\varepsilon}_{\theta r} = \frac{\partial \dot{u}_r}{\partial \theta} + \frac{\partial \dot{u}_\theta}{\partial r}, \quad \dot{\gamma}_{r\phi} = 2\dot{\varepsilon}_{r\phi} = 2\dot{\varepsilon}_{\phi r} = \frac{1}{r} \left(\frac{\partial \dot{u}_r}{\partial \theta} - \dot{u}_\theta \right) + \frac{\partial \dot{u}_\phi}{\partial r}$$

and 13

$$\dot{\gamma}_{\theta\phi} = 2\dot{\varepsilon}_{\theta\phi} = 2\dot{\varepsilon}_{\phi\theta} = \frac{1}{r} \frac{\partial \dot{u}_\phi}{\partial \theta} + \frac{\partial \dot{u}_\theta}{\partial \phi}$$

For the case of purely axisymmetric deformation, $\dot{u}_\phi = 0$ and $\partial \dot{u}_r / \partial \theta = \partial \dot{u}_\theta / \partial r = 0$, so these results simplify to the familiar expressions

$$\dot{\varepsilon}_{rr} = \frac{\partial \dot{u}_r}{\partial r}, \quad \dot{\varepsilon}_{\theta\theta} = \frac{\partial \dot{u}_\theta}{\partial \theta}, \quad \dot{\varepsilon}_{\phi\phi} = \frac{\dot{u}_r}{r}$$

1.2.1-9

4 总结与启示 1

4.1 主要研究发现 当前世界各国政府高度重视 2

CSSCI 期刊上发表的 395 篇人工智能政策研究文献 3

行系统梳理和比较分析,识别了人工智能政策研究的发展应用状况,挖掘了中外人工智能政策研究的热点主题及演进特征(如表 2 所示)。概括而言,本文得出的主要研究结论包括:

表 2 中外人工智能政策研究特征之比较

维度	国外	国内
时间跨度	1982-2020 年(研究起步较早)	2017-2020 年(近几年逐渐兴起)
应用领域	教育、医疗、就业、自动驾驶汽车等多个方面	教育、社会治理、产业以及税收政策等
主题特征	包括知识管理、流行科学、智慧城市、语言编程、就业等十二类热点主题	包括国家治理背景下人工智能政策发展路径、人工智能政策应用领域、人工智能政策文本量化分析等三类热点主题
演进趋势特征	第一,人工智能政策研究从早期初步探索利用仿真技术到通过智能化系统的改进及嵌入健康领域的应用; 第二,人工智能政策研究的重点研究方向之一是对人类的健康治理问题,包括通过人工智能方式改善心理健康服务模式; 第三,人工智能政策研究强调在系统建设的同时,需要引入人工干预措施,并强调对社会领域的影响效果	人工智能政策研究从初步的理论探索向务实应用领域的深入拓展,主要体现在两个方面:一是人工智能政策与国家、社会治理的互动关系,以及人工智能的伦理规范;二是人工智能在教育、产业、税收等领域的深入应用,以及对未来人才培养、技术进步等产生的显著影响。

首先,从研究的时间跨度可以看出,国外文献较早 4

地开启了对人工智能及人工智能政策的探索研究,尤其是 21 世纪以来国外围绕人工智能政策的研究出现了持续平稳增长态势,近三年来的发文数量更是呈现急速增长。而国内围绕人工智能政策的研究从 2017 年才刚刚开始,但是持续保持较高的研究热度。其次,从应用领域也可以看出,国外人工智能政策涉及面更广,主要集中在教育、医疗、就业等多个领域,而国内主要集中在教育、社会治理及产业、税收政策等方面。再次,从研究主题和演进趋势特征可以看出,国外人工智能政策研究主题较为丰富,主要涉及知识管理、流行科学、智慧城市等十二类热点主题,而国内研究当前主要聚焦于国家治理背景下人工智能政策发展路径、人工智能政策应用领域、人工智能政策文本量化分析等三个方面。另外,研究的演进趋势反映出国外人工智能政策研究主要沿着三条路径进行发展,而国内人工智能政策研究是从初步的理论探索向着实践应用领域进行深入拓展,可细分为两个发展方向。

4.2 针对国内研究的启示 我国人工智能政策研究 5

究起步较晚然而发展势头迅猛,通过对当前中外人工智能政策研究文献进行深入细致的比较分析,可以为国内人工智能政策研究的未来发展提供以下启示:

第 1,加快形成和构建人工智能政策研究的理论 6

框架体系。国家近三年来出台的人工智能政策数量密集,这体现了国家对人工智能当前和今后发展的高度重视。在此背景下,国内学界对人工智能研究热情高涨,然而当前围绕人工智能政策研究的成果数量非常有限。人工智能政策研究是一个亟待破解的“黑箱”,与教育、产业、医疗、文化等各个领域息息相关,尽管国内学者对这些问题展开了初步探索,但是研究内容 7

为学散缺乏系统性,而且尚未形成对人工智能政策理论框架体系的构建。因此,倘若要推动实践中人工智能政策的持续长久发展,那么势必需要尽快形成人工智能政策研究的理论框架,这一框架应该按照政策实施动因→发展路径→影响后果的因果链关系对人工智能政策研究的核心问题及基础部件进行层层廓清,以科学指导现实实践。

第 2,强化对人工智能应用领域当前和未来发展 8

的深度政策调研。人工智能可谓是推动社会经济快速发展的“万金油”,在众多行业和产业中得到了积极推广应用,但是一些学者所普遍担忧的是如何化解人工智能在现实应用中存在的诸多风险和隐患。当前国家和地方大力推广人工智能的积极应用,但是针对人工智能应用发展前景的深度政策调研尚显不足,而且国内学者围绕现有政策文本的分析更多是基于政策工具的分析视角,数据大多来源于当前网站公布的各类二手信息资料,缺乏对现实中人工智能政策领域的一手深度调研。因此,为了尽可能规避当前和未来人工智能应用过程中存在的诸多风险问题,当其所承担的就是需要强化目前人工智能政策应用现状进行深度调研和访谈,以获取更多宝贵信息,正确指引行业和产业的发展方向,充分发挥出人工智能的技术优势。

第 3,实现人工智能政策研究与国家治理之间的 9

深度融合。人工智能政策研究根植于国家现实发展战略,随着当前国家治理现代化进程的不断深入拓展,人工智能政策与环境生态保护、政府治理、教育改革、产业发展等之间的关系变得愈加紧密。与国外相比,当前国内人工智能政策在国家治理方面的应用还处于探索阶段,在很多领域还没有真正开始实施。因此,当前

Fig. A5 DocBench-100 (regular subset) — Example A. A standard single/double-column page illustrating the method's stability on common business and academic layouts.

黄冈市 2022 年高三年级 9 月调研考试 1

数学 2

本试卷共 4 页, 22 题, 全卷满分 150 分, 考试用时 120 分钟。 3

注意事项: 4

- 答卷前, 考生务必将自己的姓名、准考证号填写在答题卡上。 5
- 回答选择题时, 用铅笔把答题卡上对应题目的答案标号涂黑, 写在试卷上无效。 6
- 考试结束后, 将本试卷和答题卡一并交回。 7
- 本试卷由 kmath.cn 自动生成。 8

得分	
阅卷人	

一、单选题: 本题共 8 小题, 每小题 5 分, 共 40 分。在每小题给出的四个选项中, 只有一项是符合题目要求的。 9

1. 若集合 $M = \{x | \ln x < 1\}$, $N = \{x | \frac{x+1}{x} < 2\}$, 则 $M \cap N =$ 10

A. $\{x | x > 1\}$ 11 B. $\{x | 1 < x < e\}$ 12 C. $\{x | x < e\}$ 13 D. \emptyset 14

答案: B [解析] 16

2. 设 $a > 0, b > 0$, 则 $a \ln a < b \ln b$ 是 $b > a > 1$ 的 () 条件 17

A. 充分不必要 B. 必要不充分 C. 充要 D. 既不充分也不必要 18

答案: B [解析] 19

3. 在 $\triangle ABC$ 中, $\angle CAB = 60^\circ, AB = 2, AC = 1, D$ 为边 BC 上一点, 且 $CD = 2BD$, 则 $|AD| =$ 20

A. $\frac{\sqrt{21}}{3}$ B. $\frac{2\sqrt{3}}{3}$ C. $\frac{\sqrt{7}}{3}$ D. $\frac{\sqrt{5}}{3}$

答案: A [解析] 21

4. 已知 $f(x) = |\lg x - c|$ 有两个不同零点 a, b , 则下列结论成立的是 22

A. $a^2 + b^2$ 最小值为 23 B. $a + b$ 最小值为 24

C. $4a^2 + b^2$ 最小值为 25 D. $a^2 + b^2 - ab$ 最小值为 26

答案: C [解析] 27

5. 已知等比数列 $\{a_n\}$ 的前 n 项和为 S_n , 若 $S_3 = 4, S_6 = 12$, 则 $S_{12} =$ 28

A. 32 B. 28 C. 48 D. 60 29

答案: D [解析] 30

6. 已知 $a = e^{-\frac{2022}{2023}}, b = \frac{1}{2022}, c = \ln \frac{2023}{2022}$, 则 a, b, c 的大小关系为 31

A. $a > b > c$ B. $a > c > b$ C. $c > a > b$ D. $b > c > a$ 32

答案: A [解析] 33

7. 已知函数 $f(x) = \sin(\omega x + \theta)$, ($\omega > 0, |\theta| < \frac{\pi}{2}$), $x = \frac{\pi}{6}$ 是 $f(x)$ 的一个极值点, $x = -\frac{\pi}{6}$ 是与其相邻的一个零点, 则 $f(\frac{\pi}{3})$ 的值为 34

A. 0 B. 1 C. -1 D. $\frac{\sqrt{2}}{2}$ 35

答案: D [解析] 36

8. 已知数列 $\{a_n\}$ 满足 $a_n \cdot (-1)^n + a_{n+2} = 2n - 1, S_{20} = 650$, 则 $a_{23} =$ 37

A. 231 B. 234 C. 279 D. 276 38

答案: B [解析] 39

得分	
阅卷人	

二、多选题: 本题共 4 小题, 每小题 5 分, 共 40 分。在每小题给出的四个选项中, 有多个选项是符合题目要求的。 40

9. 下列区间中能使命函数 $y = \lg(x^3 - x^2 - x + 1)$ 单调递增的是 41

A. $[-1, +\infty)$ B. $(2, +\infty)$ C. $(-\frac{1}{3}, \frac{1}{3})$ D. $(-\frac{1}{3}, -\frac{1}{2})$ 42

答案: BD [解析] 43

10. 下列各式中, 值为 $\sqrt{3}$ 的是 44

A. $45 \cos^2 \frac{\pi}{12} - \cos^2 \frac{5\pi}{12}$ 46 B. $\frac{1 + \tan 15^\circ}{1 - \tan 15^\circ}$ 50

C. $4\sqrt{15} - \sqrt{3} \sin 15^\circ$ 48 D. $16 \sin 10^\circ \cos 20^\circ \cos 30^\circ \cos 40^\circ$ 51

答案: ABD [解析] 49

11. 在平面四边形 $ABCD$ 中, $\vec{AB} \cdot \vec{BC} = 0, \vec{AD} \cdot \vec{CD} = 0, |\vec{AB}| = |\vec{AD}| = 1, \vec{BA} = \frac{1}{2} \vec{CD}$, 若点 E 为线段 CD 上的动点, 则 $\vec{AE} \cdot \vec{BE}$ 的值可能为 52

A. 1 B. $\frac{21}{16}$ C. 2 D. $\frac{7}{2}$ 53

答案: BC [解析] 54

12. 已知函数 $y = f(x)$ 对于任意的 $x \in (0, \frac{\pi}{2})$, 均满足 $f'(x) \cos x + f(x) \sin x = \ln x$, 其中 $f'(x)$ 是 $f(x)$ 的导函数, 则下列不等式成立的是 55

A. $56(\frac{\pi}{6}) > \sqrt{3}f(\frac{\pi}{4})$ 57 B. $58(\frac{\pi}{12}) > (\sqrt{3} + 1)f(\frac{\pi}{4})$ 59

C. $60 - 1)f(\frac{\pi}{3}) < \sqrt{2}f(\frac{5\pi}{12})$ 61 D. $62 - 1)f(\frac{\pi}{3}) > \sqrt{2}f(\frac{5\pi}{12})$ 63

答案: ABC [解析] 64

得分	
阅卷人	

数学试题第 1 页 (共 6 页)

数学试题第 2 页 (共 6 页)

Fig. A6 OmniDocBench (complex) — Example A. A multi-column page with captions and side notes; geometry-aware matching preserves inter-column flow and caption linkage, illustrating robustness on challenging document layouts.

题型方法

一、常用统计量的计算

例1 (2019吉林长春,19.7分)网上学习越来越受学生的喜爱...

Table with 3 columns: 组别, 人数, 学习时间. Includes sample mean, median, and mode data.

根据以上信息,解答下列问题:

- (1)上表中的中位数m的值为... (2)用样本中的平均数估计该校七年级学生平均每人一学期(按18周计算)网上学习的时间...

解: (1)把20个数据从小到大排列,求出中间两个数的平均数,即为中位数...

解: (2)先计算该校七年级学生平均每人一学期(按18周计算)网上学习的时间为43.2小时...

解: (3)每周网上学习时间超过2小时的学生人数为130人...

解: 求一组数据的平均数、中位数、众数,要严格按照其定义进行计算...

针对训练1 (2020河南,17.9分)为发展乡村经济某村根据本地特色,创办了山药粉加工厂...

对这两台机器分装的成品进行了抽样分析,过程如下:

Table showing sample data for two machines (甲 and 乙) with columns for weight and frequency.

【整理数据】整理以上数据,得到每袋质量x(g)的频数分布表:

Frequency distribution table for machine weights with columns for weight ranges and frequencies.

【分析数据】根据以上数据,得到以下统计量:

根据以上信息,回答下列问题:

- (1)表格中的a=..., b=... (2)综合上表中的统计量,判断工厂应选购哪一台分装机,并说明理由.

解: (1)把乙组数据按从小到大的顺序排列... (2)工厂应选购乙分装机...

理由如下:比较甲、乙两台机器的统计量可知,甲与乙的平均数相同,中位数相差不大,乙的方差较小,且不合格率更低...

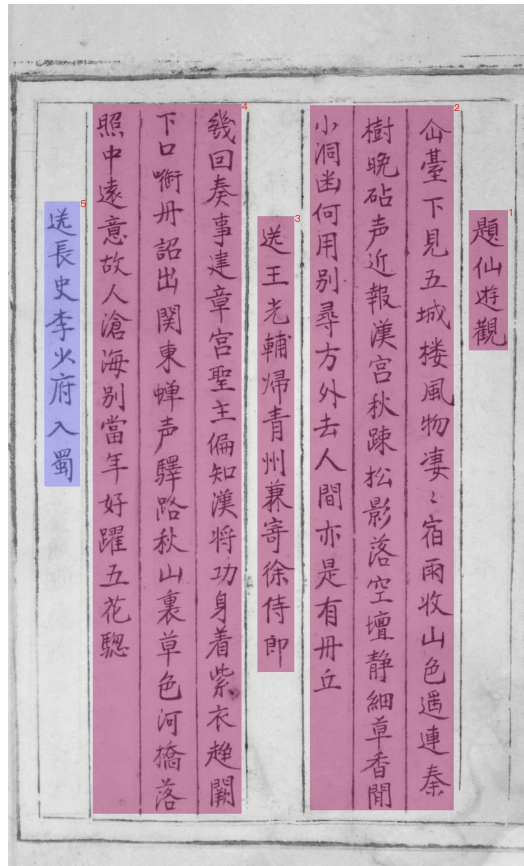


Fig. A7 OmniDocBench (double) — Example B and ancient-text case. Despite right-to-left script conventions and sparse annotations, the method maintains correct block-level order, evidencing robustness to atypical typography.

A.2 Failure Cases

7.8 Solving Systems with Cramer's Rule. A collection of 10 math problems (55-64) involving systems of linear equations and word problems. Includes a table of determinants and a list of learning objectives.

“十三五”,我们这样走过. An infographic and text block summarizing China's economic and social achievements from 2016 to 2020. Includes statistics on GDP, foreign investment, and poverty alleviation.

外商愿意来、留得住、能发展. 营商环境越来越好. A vertical text block discussing the improvement of the business environment in China, with a sub-header '营商' and a sub-sub-header '环境'.

Fig. A8 Challenging cases on OmniDocBench and DocBench-100. Failures stem from (1) insufficient fine-grained semantics and (2) sub-page complexity, leading to the sorting errors; these motivate sub-page detection and stronger semantic priors.

References

- [1] Ha J, Haralick RM, Phillips IT (1995) Recursive xy cut using bounding boxes of connected components. In: Proceedings of 3rd International Conference on Document Analysis and Recognition, IEEE, pp 952–955
- [2] Wang Z, Xu Y, Cui L, et al (2021) Layoutreader: Pre-training of text and layout for reading order detection. In: Proceedings of the 2021 Conference on Empirical Methods in Natural Language Processing, pp 4735–4744
- [3] Ouyang L, Qu Y, Zhou H, et al (2024) Omnidocbench: Benchmarking diverse pdf document parsing with comprehensive annotations. arXiv preprint arXiv:241207626
- [4] Li M, Xu Y, Cui L, et al (2020) Docbank: A benchmark dataset for document layout analysis. In: Proceedings of the 28th International Conference on Computational Linguistics, International Committee on Computational Linguistics
- [5] Zhong X, Tang J, Yepes AJ (2019) Publaynet: largest dataset ever for document layout analysis. In: 2019 International conference on document analysis and recognition (ICDAR), IEEE, pp 1015–1022
- [6] Meunier JL (2005) Optimized xy-cut for determining a page reading order. In: Eighth International Conference on Document Analysis and Recognition (ICDAR'05), IEEE, pp 347–351
- [7] Sutheebanjard P, Premchaiswadi W (2010) A modified recursive xy cut algorithm for solving block ordering problems. In: 2010 2nd International Conference on Computer Engineering and Technology, IEEE, pp V3–307
- [8] Xu Y, Li M, Cui L, et al (2020) Layoutlm: Pre-training of text and layout for document image understanding. In: Proceedings of the 26th ACM SIGKDD international conference on knowledge discovery & data mining, pp 1192–1200
- [9] Xu Y, Xu Y, Lv T, et al (2021) Layoutlmv2: Multi-modal pre-training for visually-rich document understanding. In: Proceedings of the 59th Annual Meeting of the Association for Computational Linguistics and the 11th International Joint Conference on Natural Language Processing (Volume 1: Long Papers), Association for Computational Linguistics
- [10] Huang Y, Lv T, Cui L, et al (2022) Layoutlmv3: Pre-training for document ai with unified text and image masking. In: Proceedings of the 30th ACM International Conference on Multimedia, pp 4083–4091
- [11] Xu Y, Lv T, Cui L, et al (2021) Layoutxlm: Multimodal pre-training for multilingual visually-rich document understanding. arXiv preprint arXiv:210408836
- [12] Gu Z, Meng C, Wang K, et al (2022) Xylayoutlm: Towards layout-aware multimodal networks for visually-rich document understanding. In: Proceedings of the IEEE/CVF conference on computer vision and pattern recognition, pp 4583–4592
- [13] Li M, Cui L, Huang S, et al (2020) Tablebank: Table benchmark for image-based table detection and recognition. In: Proceedings of the Twelfth Language Resources and Evaluation Conference, pp 1918–1925
- [14] Zhang J, Peng D, Liu C, et al (2024) Docres: a generalist model toward unifying document image restoration tasks. In: Proceedings of the IEEE/CVF Conference on Computer Vision and Pattern Recognition, pp 15654–15664
- [15] Yu F, Wang D, Shelhamer E, et al (2018) Deep layer aggregation. In: Proceedings of the IEEE conference on computer vision and pattern recognition, pp 2403–2412
- [16] Ma K, Shu Z, Bai X, et al (2018) Docunet: Document image unwarping via a stacked u-net. In: Proceedings of the IEEE conference on computer vision and pattern recognition, pp 4700–4709
- [17] Xu Y, Li M, Cui L, et al (2021) Layoutlmv2: Multi-modal pre-training for visually-rich document understanding. In: Proceedings of the 59th Annual Meeting of the Association for Computational

Linguistics and the 11th International Joint Conference on Natural Language Processing (Volume 1: Long Papers), pp 3452–3464

- [18] Zhou X, Yao C, Wen H, et al (2017) East: An efficient and accurate scene text detector. In: Proceedings of the IEEE Conference on Computer Vision and Pattern Recognition, pp 2642–2651
- [19] Sun T, Cui C, Du Y, et al (2025) Pp-doclayout: A unified document layout detection model to accelerate large-scale data construction. arXiv preprint arXiv:250317213
- [20] Wang B, Xu C, Zhao X, et al (2024) Mineru: An open-source solution for precise document content extraction. arXiv preprint arXiv:240918839
- [21] Papineni K, Roukos S, Ward T, et al (2002) Bleu: a method for automatic evaluation of machine translation. In: Proceedings of the 40th annual meeting of the Association for Computational Linguistics, pp 311–318